We are IntechOpen, the world's leading publisher of Open Access books Built by scientists, for scientists

4,800
Open access books available

122,000
International authors and editors

135M
Downloads

Our authors are among the

154
Countries delivered to

TOP 1%
most cited scientists

12.2%
Contributors from top 500 universities

CLARIVATE ANALYTICS BOOK CITATION INDEX INDEXED

WEB OF SCIENCE™

Selection of our books indexed in the Book Citation Index in Web of Science™ Core Collection (BKCI)

Interested in publishing with us?
Contact book.department@intechopen.com

Numbers displayed above are based on latest data collected.
For more information visit www.intechopen.com

17

Designs of True-Time-Delay Lines and Phase Shifters Based on CRLH TL Unit Cells

J. Zhang, S.W. Cheung and T.I. Yuk
Department of Electrical and Electronic Engineering,
The University of Hong Kong, Hong Kong,
China

1. Introduction

1.1 Brief description on definition of electromagnetic metamaterials

Electromagnetic (EM) Metamaterials have specific EM properties that cannot be found in nature (Caloz & Itoh, 2006). These specific EM properties are obtained by the artificial structures, rather than the composition of the metamaterials, and affect the propagations of EM waves when the average structure sizes are much smaller than the guided wavelengths λ_g, i.e., at least smaller than $\lambda_g/4$. Since the propagation of an EM wave is related to its electric and magnetic fields, the EM properties of Electromagnetic (EM) Metamaterials can be described by using its permittivity ε and permeability μ.

Fig. 1 shows the four possible combinations of permittivity and permeability of materials. In quadrant I, we can find materials such as isotropic dielectrics which have $\varepsilon > 0$ and $\mu > 0$. In quadrant II, where $\varepsilon < 0$ and $\mu > 0$, we can find materials like plasmas to have such properties. While in quadrant IV, we also can find ferromagnetic materials to have $\varepsilon > 0$ and $\mu < 0$. However, in quadrant III where both permittivity and permeability are negative, i.e. $\varepsilon < 0$ and $\mu < 0$, there is no natural material having such properties. However, one can construct artificial structures that have negative permittivity and permeability, and these artificial materials are called left-handed (LH) materials as will be explained in the following sections.

1.2 Left-handed (LH) materials

When an EM wave propagates in a conventional material, the electric field **E** and magnetic field **H** are orthogonal to each other and also orthogonal to the wave-vector **k** which has the same direction as the power flow density (also known as Poynting vector **S**). These three vectors, **E**, **H** and **k**, form a right-hand (RH) triplet, so conventional materials can also be called right-handed (RH) materials. In the 1960s, Russian physicist Viktor Veselago theoretically investigated the existence of materials with negative permittivity ε and also negative permeability μ (Veselago, 1968). He speculated that such materials would also satisfy Maxwell's equations but allow the electric field **E**, magnetic field **H** and wave-vector **k** of an EM wave to form a left-handed (LH) triplet. For this reason, the term 'left-handed' was used to describe these theoretical materials. Based on the fact that, in these materials, **E**,

H and **k** formed a LH triplet and **E**, **H** and **S** formed a RH triplet, Veselago showed that, for a uniform plane wave propagating in such materials, the direction of the wave vector **k** would be anti-parallel to the direction of the Poynting vector **S**. The phenomenon is in contrary to the case of plane wave propagation in conventional or RH materials.

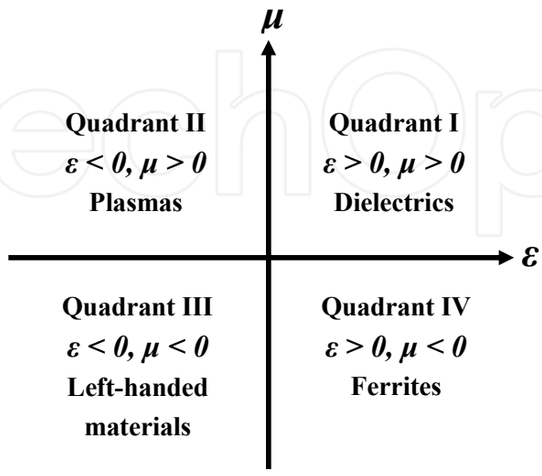

Fig. 1. Permittivity-permeability diagram

1.3 Wave propagation in LH materials by Maxwell's equations

The general form of time-varying Maxwell's equations can be written as (Ulaby, 2004):

$$\nabla \times \mathrm{E} = -\frac{\partial \mathrm{B}}{\partial t} \tag{1a}$$

$$\nabla \times \mathrm{H} = \mathrm{J} + \frac{\partial \mathrm{D}}{\partial t} \tag{1b}$$

$$\nabla \bullet \mathrm{D} = \rho \tag{1c}$$

$$\nabla \bullet \mathrm{B} = 0 \tag{1d}$$

where ∇ : vector operator $\frac{\partial}{\partial x}\hat{\mathrm{x}} + \frac{\partial}{\partial y}\hat{\mathrm{y}} + \frac{\partial}{\partial z}\hat{\mathbf{z}}$,

- $\bullet$: vector dot product,
- **E:** electric field intensity, in V/m,
- **H:** magnetic field intensity, in A/m,
- **D:** electric flux density, in C/m^2,
- **B:** magnetic flux density, in W/m^2,
- **J:** electric current density, in A/m^2, and
- ρ : electric charge density, in C/m^3.

The relationships between the field intensities **E** and **B,** flux densities **D** and **H** and current density **J** are (Ulaby, 2004):

$$\mathrm{D} = \varepsilon \mathrm{E}, \quad \mathrm{B} = \mu \mathrm{H}, \quad \mathrm{J} = \sigma \mathrm{E} \tag{2}$$

where ε, μ and σ are the electric permittivity (also called the dielectric constant), permeability and conductivity, respectively, of the material under consideration.

Consider a wave having a single frequency ω. Then by introducing the time factor $e^{+j\omega t}$ to (1), the time derivatives in Maxwell's equations of (1) can be replaced by $j\omega$ and Maxwell's equations can be re-written as:

$$\nabla \times \mathrm{E} = -j\omega\mu \mathrm{H} \tag{3a}$$

$$\nabla \times \mathrm{H} = (\sigma + j\omega\varepsilon)\mathrm{E} \tag{3b}$$

$$\nabla \bullet \mathrm{E} = \rho / \varepsilon \tag{3c}$$

$$\nabla \bullet \mathrm{H} = 0 \tag{3d}$$

In free space which is lossless, J, σ and ρ are all zero and (3) becomes:

$$\nabla \times \mathrm{E} = -j\omega\mu \mathrm{H} \tag{4a}$$

$$\nabla \times \mathrm{H} = j\omega\varepsilon \mathrm{E} \tag{4b}$$

$$\nabla \bullet \mathbf{E} = 0\rho / \varepsilon \tag{4c}$$

$$\nabla \bullet \mathrm{H} = 0 \tag{4d}$$

It can be readily shown from (4) that

$$\nabla^2 \mathrm{E} + k^2 \mathrm{E} = 0 \tag{5a}$$

$$\nabla^2 \mathrm{H} + k^2 \mathrm{H} = 0 \tag{5a}$$

where $k = 2\pi/\lambda$ is the wave number (which is real if ε and μ are real) with λ being the wavelength.

(5) is known as the wave equation which has many solutions. A plane wave is a wave having a constant phase over a set of planes, while a uniform-plane wave is a wave having both magnitude and phase constant. An EM wave in free space is a uniform-plane wave having the electric field **E** and magnetic field **B** mutually perpendicular to each other and also to the direction of propagation, i.e., a transverse electromagnetic (TEM) wave. For convenience and without lost of generality, assume that the EM wave considered is propagating in the +z direction in free space. Under these conditions, the solution for (5) is (Ulaby, 2004):

$$\mathrm{E}(z) = \mathrm{E}_0 e^{-j\,\mathrm{k}\bullet\mathbf{z}} \tag{6a}$$

$$\mathrm{H}(z) = \mathbf{e}_\mathbf{k} \times \frac{1}{\eta_0}\mathrm{E}(z) = \frac{\mathbf{e}_\mathbf{k} \times \mathrm{E}_0(z)}{\eta_0} e^{-j\,\mathrm{k}\bullet\mathbf{z}} \tag{6b}$$

where $\mathbf{E}_0 = E_m e^{j\phi}\mathbf{e}_x$ (with $E_m = |\mathbf{E}_0|$ and $\mathbf{e}_x$ being the unit vector along +x direction)
- η_0 : free space impendence 377 Ω
- **k**: wave vector having magnitude of k at **+z** direction .

Substituting (6a) and (6b) into (4a) and (4b), respectively, yields

$$\mathrm{k}\times\mathrm{E} = \omega\mu\mathrm{H} \tag{7a}$$

$$\mathrm{k}\times\mathrm{H} = -\omega\varepsilon\mathrm{E} \tag{7b}$$

in which, for positive values of ε and μ, the triplet (**E**, **H**, **k**) can be used to produce an orthogonality diagram shown in Fig. 2(a) using our right hand (RH). However, if ε and μ are both negative, (7) becomes:

$$\mathrm{k}\times\mathrm{E} = -\omega|\mu|\mathrm{H} \tag{8a}$$

$$\mathrm{k}\times\mathrm{H} = \omega|\varepsilon|\mathrm{E} \tag{8b}$$

in which now the triplet (**E**, **H**, **k**) forms an orthogonality diagram shown in Fig. 2(b) using our left hand (LH). This result verifies Velago's speculation and this is the primary reason for materials with negative ε and μ to be called LH materials.

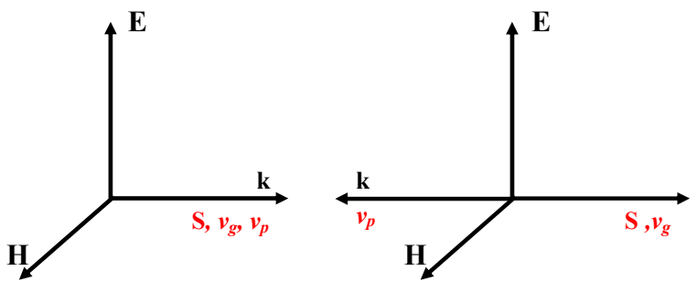

(a) (b)

Fig. 2. Orthogonality diagram of E, H, k for uniform plane wave in (a) RH material and (b) LH material

The power flow density of an EM wave, also known as the Poynting vector, is defined as (Ulaby, 2004):

$$\mathrm{S} = \mathrm{E}\times\mathrm{H} \tag{9}$$

(9) indicates that the power flow density is only determined by **E** and **H** but not the signs of ε and μ. Thus in both RH and LH materials, the triplets (**E**, **H, S)** have the same form of orthogonality, i.e., following our right hand, as shown in Figs. 2(a) and 2(b), and the directions of energy flow are the same.

The group velocity v_g of an EM wave is given by (Ulaby, 2004):

$$v_g = \frac{\partial \omega}{\partial k} \tag{10}$$

which expresses the velocity of power flow and so has the same direction as the Poynting vector **S**, as shown in Fig. 2.

The phase velocity v_p is the velocity of wave-front given by (Ulaby, 2004):

$$v_p = \frac{\omega}{k} \tag{11}$$

and so has the same sign as k, i.e., $v_p > 0$ for $k > 0$ in RH materials and $v_p < 0$ for $k < 0$ in LH materials. As a result, the v_p in LH materials and in RH materials are anti-parallel as indicated in Fig. 2.

Table 1 summarizes the aforementioned analysis for a plane uniform EM wave in the RH and LH materials.

	triplet **(E,H,k)**	k	v_p	triplet **(E,H,S)**	v_g
RH material	RH orthogonality	> 0	> 0	RH orthogonality	> 0
LH material	LH orthogonality	< 0	< 0	RH orthogonality	> 0

Table 1. Characteristics of RH and LH material

2. Transmission line (TL) approach of metamaterials

2.1 Left-handed transmission lines (LH TLs)

A microstrip transmission line fabricated on a substrate is shown in Fig. 3(a). The transmission line is also called a right-handed transmission line (RH TL) because when an EM wave travelling through it, the triplet (**E, H, k**) forms a RH orthogonality, as will be shown later. The equivalent circuit of the transmission line is shown in Fig. 3(b), where L_R models the RH series inductance along the transmission line and C_R models the RH shunt capacitance between the transmission line and the ground on the other side of the substrate (Pozar, 2004).

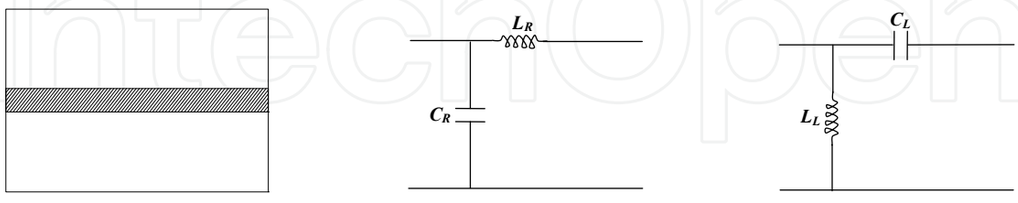

(a) (b) (c)

Fig. 3. (a) Structure of RH TL (b) equivalent circuit of RH TL and (c) equivalent circuit of LH TL

To simplify our analysis, we assume that the transmission line is lossless. The complex propagation constant γ, the phase constant β, the phase velocity v_p and the group velocity v_g of the RH TL are, respectively, given by (Pozar, 2004):

$$\gamma = j\beta = \sqrt{ZY} = j\omega\sqrt{L_R C_R} \tag{12a}$$

$$\beta = \omega\sqrt{L_R C_R} > 0 \tag{12b}$$

$$v_p = \frac{\omega}{\beta} = \frac{1}{\sqrt{L_R C_R}} > 0 \tag{12c}$$

$$v_g = \frac{\partial\omega}{\partial\beta} = \frac{1}{\sqrt{L_R C_R}} > 0 \tag{12d}$$

By making a duality of the equivalent circuit in Fig. 3(b), i.e. replacing the series inductance L_R with a series capacitance C_L and the shunt capacitance C_R with a shunt inductance L_L, we can have the equivalent circuit of a left-handed transmission line (LH TL) (Lai et al., 2004) shown in Fig. 3(c). It is called a LH TL simply because when an EM wave travelling through it, the triplet (**E, H, k**) forms a LH orthogonality, as will be shown later. Now the complex propagation constant γ, the phase constant β, the phase velocity v_p and the group velocity v_g of the LH TL can be found as

$$\gamma = j\beta = \sqrt{ZY} = -j\omega\frac{1}{\sqrt{L_L C_L}} \tag{13a}$$

$$\beta = -\frac{1}{\omega\sqrt{L_L C_L}} < 0 \tag{13b}$$

$$v_p = \frac{\omega}{\beta} = -\omega^2\sqrt{L_L C_L} < 0 \tag{13c}$$

$$v_g = \frac{\partial\omega}{\partial\beta} = \omega^2\sqrt{L_L C_L} > 0 \tag{13d}$$

Here the phase constant β (= $2\pi/\lambda$) in (13b) (equivalent to the wave number k used in wave propagation previously) is negative and so the phase velocity v_p in (13c) associated with the direction of phase propagation is negative. However, the group velocity v_g in (13d) indicating the direction of power flow (Poynting vector S) remains positive. This characteristic agrees with that of LH materials shown in Table 1, so the LC circuit shown in Fig. 3(c) can be used to realize LH materials.

2.2 Composite right/left-handed transmission line (CRLH TL)

The transmission line structure shown in Fig. 4(a) was proposed in (Lai et al., 2004) to realize the series capacitance C_L and shunt inductance L_L in Fig. 3(c) for the LH materials (Lai et al., 2004). The structure consists of a series inter-digital capacitors to realize the series capacitance C_L and a via shunted to ground on the other of the substrate to realize the shunt inductance L_L. However, when an EM wave travels along the structure, the current flowing along the upper metal trace induces a magnetic field, creating an inductive effect. This effect

is modeled by the series inductance L_R in Fig. 4(b). Moreover, the potential difference generated between the upper metal trace and the ground plane on the other side produces an electric field, creating a capacitive effect. This effect is modeled by the shunt capacitance C_R in Fig. 4(b). Since the inductive and capacitive effects caused by the series inductance L_R and shunt capacitance C_R, respectively, cannot be avoided in practical implementation of LH TLs, the term "composite right/left-handed transmission line" (CRLH TL) is used to describe such a structure.

(a) (b)

Fig. 4. (a) CRLH TL structure and (b) equivalent circuit

2.3 Dispersion diagrams

Here, we show that the structure of Fig. 4(a) indeed has LH and RH properties shown in Table 1. The complex propagation constant of the CRLH TL structure in Fig. 4(b) can be written as (Caloz & Itoh, 2006; Lai et al., 2004)

$$\gamma = \alpha + j\beta = \sqrt{ZY} \tag{14}$$

where α and are β are the attenuation and phase constants, respectively. Assume the structure, as represented by Fig. 4(a), is lossless,and so has no attenuation, i.e. $\alpha = 0$ in (14). The propagation constant is an imaginary number:

$$\gamma = j\beta = \sqrt{ZY} = \sqrt{(j\omega L_R + \frac{1}{j\omega C_L})(j\omega C_R + \frac{1}{j\omega L_L})} \tag{15a}$$

$$= \sqrt{(-1)}\sqrt{\omega^2 L_R C_R + \frac{1}{\omega^2 L_L C_L} - (\frac{L_R}{L_L} + \frac{C_R}{C_L})} \tag{15b}$$

$$= js(\omega)\sqrt{\omega^2 L_R C_R + \frac{1}{\omega^2 L_L C_L} - (\frac{L_R}{L_L} + \frac{C_R}{C_L})} \tag{15c}$$

where

$$s(\omega) = \pm 1 \tag{16}$$

In the equivalent circuit of Fig. 4(b), the components C_L and L_R form a series-tune circuit with a resonant frequency at $1/\sqrt{L_R C_L}$. At frequencies larger than $1/\sqrt{L_R C_L}$, the circuit is inductive. While the components C_R and L_L form a parallel-tune circuit resonating at $1/\sqrt{L_L C_R}$. At frequencies larger than $1/\sqrt{L_L C_R}$, the circuit is capacitive. Thus, at frequencies $\omega > \max(1/\sqrt{L_R C_L}, 1/\sqrt{L_L C_R})$, the series-tune circuit is inductive and the parallel-tune circuit is capacitive. The CRLH TL structure will have an equivalent-circuit model similar to one shown in Fig. 3(b) and so behaves like a RH TL. Under this condition, from (12b), the propagation constant is a positively imaginary number, i.e., $\gamma = j\beta$, and so $s(\omega) = +1$ in (16). At frequencies less than $1/\sqrt{L_R C_L}$, the series-tune circuit formed by C_L and L_R is capacitive. At frequencies less than $1/\sqrt{L_L C_R}$, the parallel-tune circuit formed by C_R and L_L is inductive. Thus at frequencies $\omega < \min(1/\sqrt{L_R C_L}, 1/\sqrt{L_L C_R})$, the series-tune circuit is capacitive and the parallel-tune circuit is inductive. Now the CRLH TL structure has an equivalent-circuit model similar to one shown in Fig. 3(c) and so behaves like a LH TL. Under this condition, from (13b), the propagation constant is a negatively imaginary number i.e., $\gamma = -j\beta$ and so $s(\omega) = -1$ in (16). Between these two limits, i.e., $\min(1/\sqrt{L_R C_L}, 1/\sqrt{L_L C_R}) < \omega < \max(1/\sqrt{L_R C_L}, 1/\sqrt{L_L C_R})$, the radicand in (15c) is purely imaginary and so the propagation constant is purely real at $\gamma = \beta$. There is only attenuation in the CRLH TL structure which behaves as a stop-band filter. This stop band is a unique characteristic of the CRLH TL.

Therefore, the propagation constant of a CRLH TL structure can be re-written from (15) as:

$$\gamma(\omega) = \begin{cases} j\beta(\omega) = j\sqrt{\omega^2 L_R C_R + \dfrac{1}{\omega^2 L_L C_L} - \left(\dfrac{L_R}{L_L} + \dfrac{C_R}{C_L}\right)} \\ \quad \text{If } \omega > \max\left(\dfrac{1}{\sqrt{L_R C_L}}, \dfrac{1}{\sqrt{L_L C_R}}\right) \\ j\beta(\omega) = -j\sqrt{\omega^2 L_R C_R + \dfrac{1}{\omega^2 L_L C_L} - \left(\dfrac{L_R}{L_L} + \dfrac{C_R}{C_L}\right)} \\ \quad \text{If } \omega < \min\left(\dfrac{1}{\sqrt{L_R C_L}}, \dfrac{1}{\sqrt{L_L C_R}}\right) \\ \beta(\omega) = \sqrt{-\omega^2 L_R C_R - \dfrac{1}{\omega^2 L_L C_L} + \left(\dfrac{L_R}{L_L} + \dfrac{C_R}{C_L}\right)} \\ \quad \text{If } \min\left(\dfrac{1}{\sqrt{L_R C_L}}, \dfrac{1}{\sqrt{L_L C_R}}\right) < \omega < \max\left(\dfrac{1}{\sqrt{L_R C_L}}, \dfrac{1}{\sqrt{L_L C_R}}\right) \end{cases} \tag{17}$$

The dispersion diagrams of the RH TL, LH TL, and CRLH TL plotted using (12b), (13b) and (17), respectively, are shown in Fig. 5 (Caloz & Itoh, 2006; Lai et al., 2004). For the RH TL, Fig. 5(a) shows that the group velocity (i.e., $v_g = d\omega/d\beta$) is positive and has values only for $\beta > 0$. Since phase velocity is defined as $v_p = \omega/\beta$, Fig. 5(a) shows that the RH TL has $v_p > 0$. Fig. 5(b) shows that the LH TL also has a positive group velocity ($v_g = d\omega/d\beta$) but only for $\beta < 0$ which leads to $v_p < 0$ (because $v_p = \omega/\beta$). These characteristics agree with those of the RH and LH materials shown in Table 1. Thus the circuit models in Figs. 3(b) and 3(c) realized using

transmission lines have the EM properties of the RH and LH materials, respectively. In Fig. 5(c), the regions for $\beta > 0$ and $\beta < 0$ are known here as the RH and LH regions, respectively.

Now, consider the dispersion diagram in Fig. 5(c). It can be seen that the CRLH TL behaves like a LH TL for $\beta < 0$ ($v_p < 0$, $v_g > 0$) and like a RH TL for $\beta > 0$ ($v_p > 0$, $v_g > 0$). Thus the circuit of Fig. 4(b) indeed has both the LH and RH properties. Fig. 5(c) shows that the CRLH TL has quite small group velocities in the LH region and much large group velocities in the RH region. The LH region with low group velocities can be used to implement TTDLs with high time-delay efficiencies as described later. Moreover, the CRLH TL has a stopband in the frequency range: $\min(1/\sqrt{L_R C_L}, 1/\sqrt{L_L C_R}) < \omega < \max(1/\sqrt{L_R C_L}, 1/\sqrt{L_L C_R})$, where $\beta = 0$, leading to a zero group velocity v_g and meaning zero power flow.

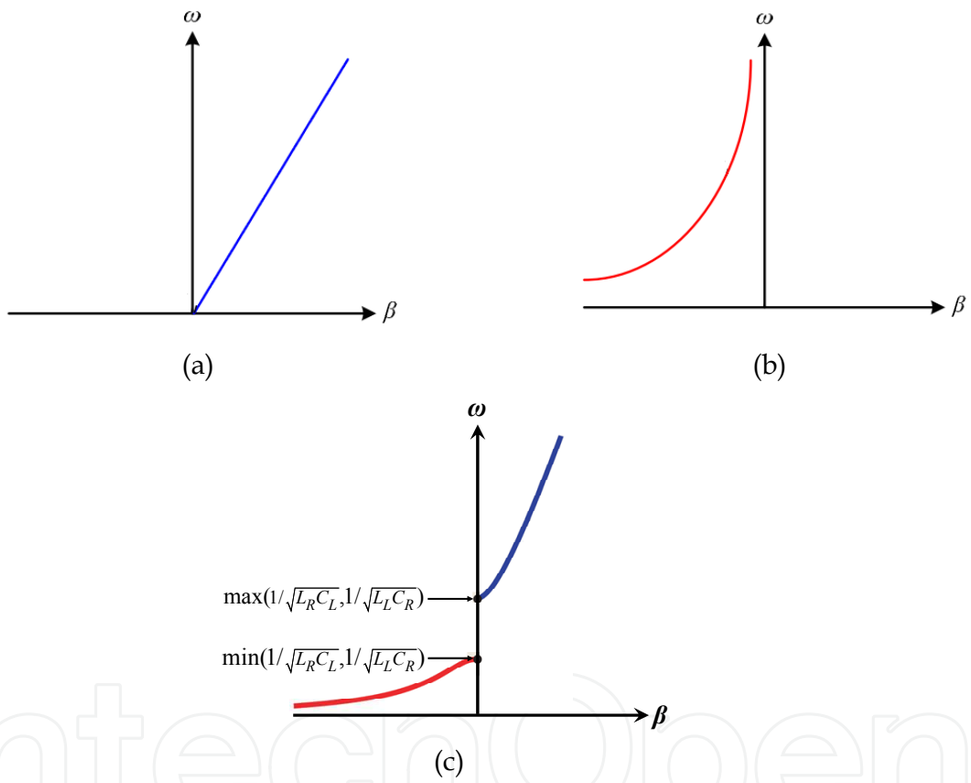

Fig. 5. Dispersion diagrams of (a) RH TL, (b) LH TL and (c) CRLH TL

3. True-time-delay lines (TTDLs) using CRLH TL unit cells

3.1 Introduction

True-time-delay lines (TTDLs) are widely employed in various microwave devices and subsystems. They find applications in phased arrays, feed-forward amplifiers, delay-lock loops, phase noise measurement systems and oscillators (Lee, 2004). There are different approaches to implement the TTDLs. For example, in magnetostatic wave (MSW) TTDLs (Fetisov & Kabos, 1998) and surface-acoustic wave (SAW) TTDLs (Smith & Gerard, 1969), the group velocities were slowed down by transferring the microwave signals into the

magnetostatic waves and surface acoustic waves, respectively. These designs have quite high time-delay efficiencies, but the bulky and complicated transducers required are not conducive for planar microwave circuits. Moreover, SAW TTDLs have extremely narrow bandwidths of only several MHz and MSW TTDLs have very large insertion losses. Optical TTDLs (Xu et al., 2004) have very small insertion losses, so we can use very long optical fiber cables to achieve very large TDs. However, optical TTDLs also need complicated transducers to transfer the microwave signals into the optical waves.

Microstrip lines, with the advantages of simplicity in feeding and compatibility with planar circuits, are widely used in communications systems, particularly for small communications devices. A simple RH TL can also be used to implement TTDL. However, due to the low time-delay efficiency, it is difficult to achieve a long TD using RH TL. To increase the time-delay efficiency of RH TL, various slow-wave structures have been proposed. Some employ periodic discontinuities such as the Electromagnetic Bandgap Structures (EBG) (Kim & Drayton, 2007) and defected ground structure (DGS) (Woo et al., 2008). Others use periodic equivalent LC networks (Zhang & Yang, 2008; Zhang et al., 2011). All of these designs adapt the same basic concept,of increasing the series inductance and shunt capacitance per unit length, hence the effective dielectric, to reduce the guided wavelength of the EM waves.

As described previously, the CRLH TL has a unique dispersion characteristic, i.e., having small group velocities in the LH region. Thus a CRLH TL operating in the LH region can be used to realize a TTDL with a high time-delay efficiency. In this section, a TTDL using four symmetrical CRLH TL unit cells is studied.

3.2 TTDL realized by transmission line (TL)

The true-time delay (TTD) of a transmission line (TL) is the time it takes for an EM wave to travel through it, so a TL can be used to design a TTDL. For a TL with a length of L, the TTD is:

$$\tau = L / v_g \tag{18}$$

where v_g is the group velocity given by

$$v_g = d\omega / d\beta \tag{19}$$

with β and ω being the propagation constant and frequency in rad/s, respectively. (18) and (19), show that the TTD is inversely proportional to the group velocity v_g. For a given length of TL, the smaller is the v_g, the longer will be the TD.

3.3 Symmetrical CRLH TL unit cell

To design a TTDL with a large TTD, we propose to cascade a number of CRLH TL structures together, each having a small group velocity. For matching purpose, the CRLH TL structure has to be designed so that S_{11} = S_{22} over the operating frequency band. However, this is not easy to do using the CRLH TL structure shown in Fig. 4(a) because adjusting any of the structural parameters will change both S_{11} and S_{22}. To overcome such difficulty, we propose a new structure as shown in Fig. 6 which has a symmetrical structure

and is here called a symmetrical CRLH TL unit cell (Zhang et al., 2009). Compared with the CRLH TL structure as shown in 4(a), our proposed CRLH TL unit cell has two stubs, instead of one stub, having a grounded via, making the whole structure centrosymmetrical. To deign such unit cell for use in our TTDL, we only need to match the input impedance to a 50-Ω coaxial cable, which is relatively easy to do. Once this matching is designed, due to its symmetrical structure, the two Z-parameters, Z_{11} and Z_{22}, will be the same and equal to 50 Ω. The symmetry of the unit cell leads to an equivalent-symmetrical π-model shown in Fig. 6(c) in which L_R models the RH series inductance along all the horizontal fingers, C_L models the LH coupling capacitance between the fingers, $2L_L$ models the LH shunt inductance of each stub having a via at the end to the ground, and $C_R/2$ models the RH shunt capacitance between the fingers and the ground on each side of the unit cell.

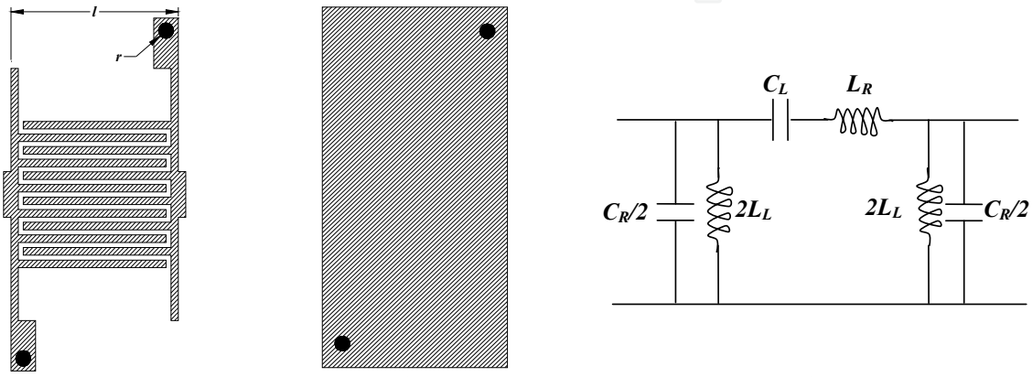

Fig. 6. Proposed CRLH TL unit cell. (a) Top view, (b) bottom, and (c) equivalent circuit.

Here, we will show that the CRLH TL unit cell in Fig. 6(a) has the same dispersion diagram shown in Fig. 5 (c), so that we can have the LH region to operate the unit cell. The expressions for L_R, C_R, L_L and C_L in Fig. 6(c) are, respectively, given by (Bahl, 2001; Marc & Robert, 1991; Pozar, 2004):

$$L_R = \frac{Z_0\sqrt{\varepsilon_{re}}}{Nc}l \tag{20a}$$

$$C_R = \frac{N\sqrt{\varepsilon_{re}}}{Z_0 c}l \tag{20b}$$

$$C_L = (\varepsilon_r + 1)l\left\{4.409(N-3)\tanh\left[0.55\left(\frac{h}{W}\right)^{0.45}\right] + 9.92\tanh\left[0.52\left(\frac{h}{W}\right)^{0.5}\right]\right\}\times 10^{-12} \tag{20c}$$

$$L_L = \frac{\mu_0}{2\pi}\left[h\cdot\ln\left(\frac{h+\sqrt{r^2+h^2}}{r}\right) + \frac{3}{2}(r-\sqrt{r^2+h^2})\right] + \frac{Z_0\sqrt{\varepsilon_{re}}}{c}l' \tag{20d}$$

where h is the thickness of the substrate, r is the radius of the ground via, ε_r is the relative dielectric constant, ε_{re} is the effective dielectric constant, l' is the distance from the ground via to the port, l is the length of the finger, N is the number of fingers, W is the width of all

the fingers together and Z_0 is the characteristic impedance of each of the fingers. To derive the complex propagation constant of this symmetrical CRLH TL unit cell, we separate the L_R and C_L in Fig. 6(c) into two capacitances $2C_L$ and two inductances $L_R/2$, respectively. This results in two sub-circuits as shown in Fig. 7, each having the same propagation constant γ'. The total propagation constant γ is the sum of the propagation constants for these two sub-circuits, i.e., $\gamma = 2\gamma'$. In Fig. 7, the propagation constant of the symmetrical CRLH TL unit cell is:

$$\gamma = j\beta = 2\gamma' = 2\sqrt{ZY} = 2\sqrt{(j\omega\frac{L_R}{2}+\frac{1}{j\omega 2C_L})(j\omega\frac{C_R}{2}+\frac{1}{j\omega 2L_L})}$$

$$= \sqrt{(-1)}\sqrt{\omega^2 L_R C_R + \frac{1}{\omega^2 L_L C_L} - (\frac{L_R}{L_L}+\frac{C_R}{C_L})}$$

$$= js(\omega)\sqrt{\omega^2 L_R C_R + \frac{1}{\omega^2 L_L C_L} - (\frac{L_R}{L_L}+\frac{C_R}{C_L})} \tag{21}$$

$$\text{where } s(\omega) = \pm 1$$

(21) shows that the propagation constant is exactly the same as (15c). Thus the symmetrical CRLH TL unit cell has the same dispersion diagram shown in Fig. 5(c).

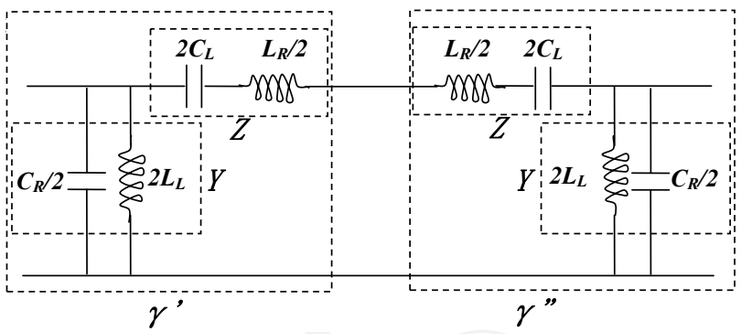

Fig. 7. Equivalent circuit of Fig. 6(c)

3.4 TTDL realization using symmetrical CRLH TL unit cells

From (18) and (19), the TD of a TL is given by

$$\tau = \frac{L}{v_g} = \frac{L}{d\omega/d\beta} = \frac{Ld\beta}{d\omega} = \frac{Ang(s_{21})}{2\pi df} \tag{22}$$

where $Ang(S_{21})$ is the phase of S_{21}. Figure 5(c) shows that the CRLH TL has quite small group velocities v_g in the LH region and much higher group velocities in the RH region. Thus the LH region with low group velocities can be used to implement TTDLs with longer TTDs and high time-delay efficiencies as indicated in (22). It can be see that (22) also indicate that, for a given length L, the larger is the slope of phase response, i.e., $Ang(S_{21})/df$, the longer will be the TD or the higher will be the time-delay efficiency. Moreover, by adjusting

L_R, C_R, L_L and C_L using the structural parameters through (20), the CRLH TL unit cell can also be designed to operate at different frequencies and TDs.

3.5 Simulation and measurement results

3.5.1 Single CRLH TL unit cell

The proposed symmetrical CRLH TL unit cell shown in Fig. 6 has been designed with a center frequency at around 3 GHz on a Rogers substrate, RO4350, with a thickness of 0.762 and a permittivity of 3.48 using computer simulation. It has a total a length of 6.8 mm. The design is optimized for the criteria for wide impedance bandwidth, small insertion and large phase response. The simulated results on return loss, -10log$|S_{11}|$, and insertion loss, -10log$|S_{21}|$, of the CRLH TL unit cell are shown in Fig. 8(a), while the phase response, (Ang(S_{21})), shown in Fig. 8(b). For comparison, the results of a RH TL with the same length of 6.8 mm are also shown in the same figure. Figure 8(a) shows that the CRLH unit cell has an operating bandwidth of 2.2-4.0 GHz, a return loss of large than 15 dB and insertion loss of less than 1 dB within the operating bandwidth. The slope of phase response, as shown in Fig. 8(b), is 41.3 degree/GHz, about 3 times larger that of the RH TL at 13.3 degree/GHz. Thus we can expect that the CRLH TL unit cell can achieve a TTD 3.1 times longer than that of a RH TL for the same length and so has the time delay efficiency 3.1 times higher than that of the RH TL.

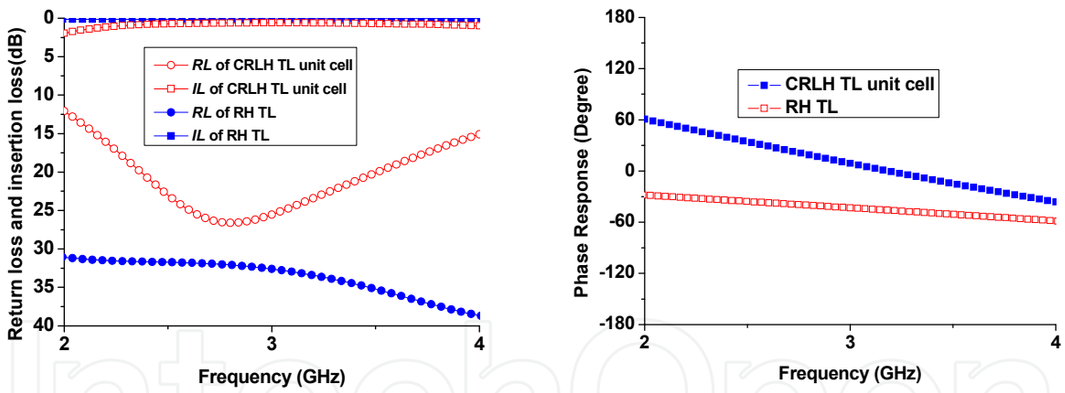

(a) (b)

Fig. 8. Simulated (a) return loss (RL) and insertion loss (IL) and (b) phase response of CRLH TL unit cell and RH TL

3.5.2 Multi-CRLH TL unit cells

A TTDL constructed by cascading four symmetrical CRLH unit cells, with a total length of 30 mm, is shown in Fig. 9(a). The TTDL has been designed, studied and optimized using computer simulation. The final design has also been implemented on a Rogers substrate, RO4350, with a thickness of 0.762 and a permittivity of 3.48 and measured for verification of simulation results. For comparison, a TTDL implemented using a RH TL with the same

length of 30 mm, as shown in Fig. 9(b), has also been designed and simulated using the same substrate. The prototype-modules of the two TTDLs with the same dimension of 30 mm×15 mm×2 mm are shown in Fig. 10.

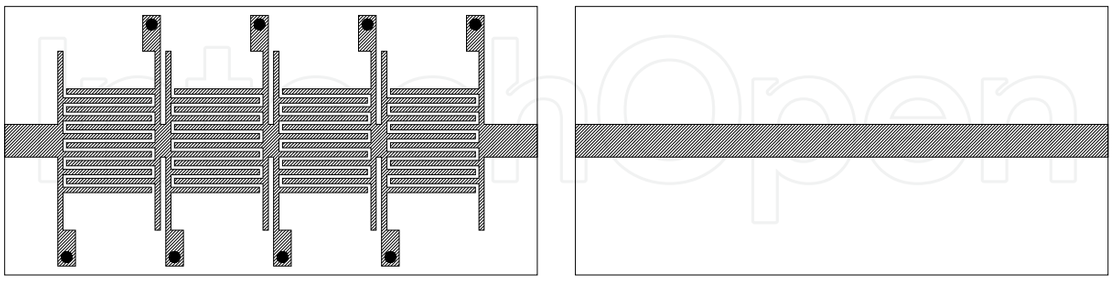

(a) (b)

Fig. 9. TTDLs using (a) four CRLH TL unit cells and (b) RH TL

(a) (b)

Fig. 10. Prototypes of TTDLs using (a) four CRLH TL unit cells and (b) RH TL

The simulated and measured return losses, insertion losses and TTDs of the two TTDLs are shown in Fig. 11. It can be seen that the simulated and measured results show good agreements. Figure 11(a) show that the measured return losses and the insertion losses of the TTDLs are more than 15 dB and less than 1 dB, respectively, across the frequency band from 2.2 – 3.7 GHz. The measurement results in Fig. 11(b) show that the TTDL using CRLH TL unit cells achieves a TTD of 510 ps, about 3.2 times larger than the RH TL having a TTD of 160 ps. This result is consistent with the result obtained for a single CRLH TL unit cell. The measurement results in Fig. 11(b) show that the maximum TTD error for the TTDL using the CRLH TL unit cells is about -21 ps or -4.1% at the frequency of 2.4 GHz. For the TTDL using RH TL, although the maximum TD error is about -7.8 ps at the frequency of 2.8 GHz, the percentage is higher at -4.8%.

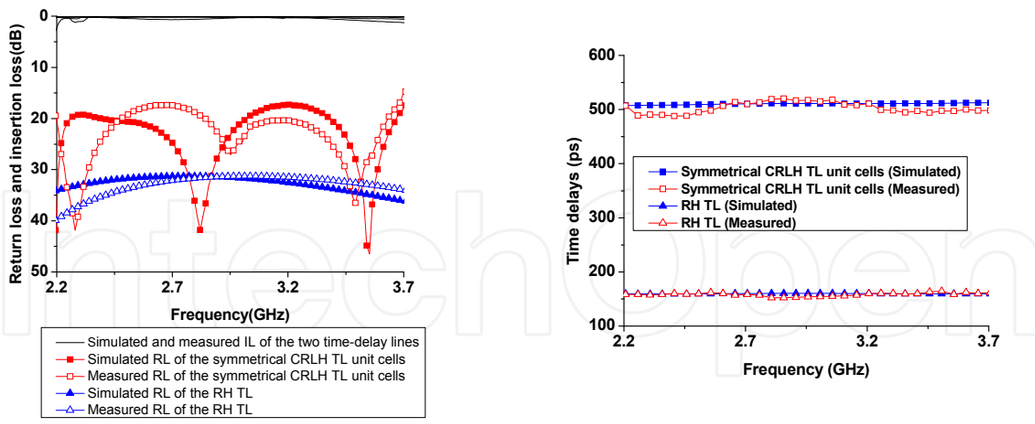

(a) (b)

Fig. 11. Simulated and measured (a) return loss and insertion loss and (b) TTDs of TTDLs using CRLH TL unit cells and RH TL

4. Digital-phase shifters using CRLH unit cells

4.1 Introduction

Phase shifters are essential components in radar and phased array systems. In the designs of phase shifters, insertion loss, size and power-handling capability are major factors for considerations. Phase shifters can be classified into passive and active. Passive phase shifters can be implemented using ferrite technology (Adam et al., 2002) to achieve higher power capabilities, but they have large sizes and heavy weights. Active phase shifters implemented using solid-state devices such as FET and CMOS technologies have smaller sizes. However, their low power-handling capabilities and nonreciprocal characteristics limit their applications.

In digital-phase shifters, phase shift is usually obtained by switching between two transmission lines of different lengths or between lumped-element low-pass and high-pass filters (Keul & Bhat, 1991). Usually, the switches are implemented using solid-state devices such as PIN diodes which have typical power-handling capabilities of just a few Watts and this limits the power-handling capabilities of the phase shifters. Moreover, if an *n*-bit phase shifter is constructed by cascading several phase shifters together to provide the required phase shifts, the physical size and insertion loss will be undoubtedly increased.

Recently, different design approaches of phase shifters based on using metamaterials have been proposed and studied (Antoniades & Eleftheriades, 2003; Damm et al., 2006; Kim et al., 2005; Kholodnyak et al., 2006; Lapine et al., 2006; Vendik et al., 2009;). These designs share one of the major drawbacks, i.e., the power-handling capability is limited by the power-handling capabilities of the switches, tunable diodes and tunable capacitors used in the designs. A phase shifter based on CRLH TL employing MEMS has also been proposed and studied (Monti et al., 2009), but the reliability of the design needs more studies (Rebeiz et al., 2002).

In this section, we present an approach for the design of *n*-bit phase shifters using the CRLH TL unit cells. The phase shifters designed using this approach have the advantages of compact size, high power-handling capability, low insertion loss, arbitrary phase-shift range and arbitrary step size. PIN diodes mounted on the fingers of the CRLH TL unit cell are used as switches to control the phase shift. Different phase shifts are achieved by using different states of these switches and the controlling bits are used to select one of those switch states for the required phase shift.

4.2 Description of CRLH TL unit cell using ABCD-parameters

The symmetrical CRLH TL unit cell used for the designs of digital-phase shifters is shown in Fig. 12(a) with the equivalent π-model circuit shown in Fig. 12(b). The symmetrical CRLH TL unit cell and the equivalent π-model circuit are similar to those shown in Fig. 6(a), thus the expressions for L_R, C_R, L_L and C_L are same as given in (20a)-(20d).

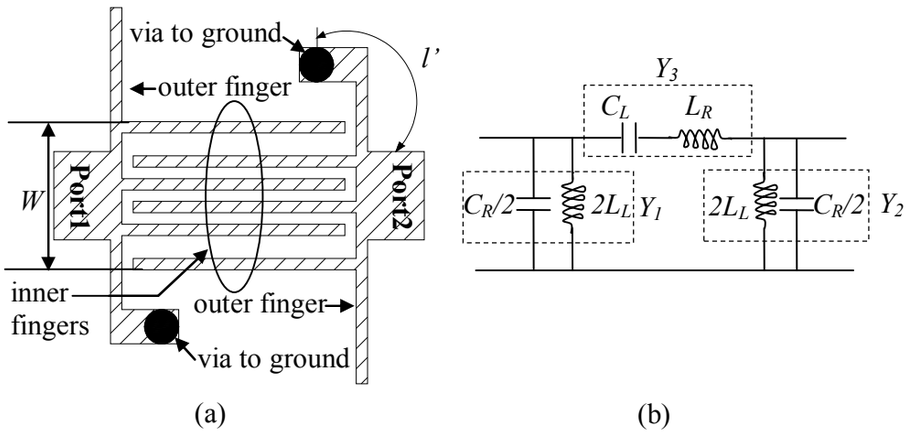

Fig. 12. Structure and equivalent circuit of symmetrical CRLH TL unit cell.

The transmission ABCD matrix of the π-model circuit in Fig. 12 (b) is (M.D. Pozar, 2004):

$$\begin{bmatrix} A & B \\ C & D \end{bmatrix} = \begin{bmatrix} 1+Y_2/Y_3 & 1/Y_3 \\ Y_1+Y_2+Y_1Y_2/Y_3 & 1+Y_1/Y_3 \end{bmatrix} \tag{23}$$

where $Y_1 = Y_2 = j\omega C_R/2 + 1/2j\omega L_L$ and $Y_3 = \dfrac{1}{j\omega L_R + 1/j\omega C_L}$.

Using (23), the expressions for S_{11}, S_{21} and phase incursion Ang(S_{21}) can be easily obtained, respectively, as:

$$S_{11} = \frac{(\frac{b}{Z_0})^2 - Z_0^2 a^2 [2-ab]^2}{4[1-ab]^2 + [Z_0 a^2 b - 2Z_0 a - (\frac{b}{Z_0})]^2} + j\frac{2[1-ab][2Z_0 a - \frac{b}{Z_0} - a^2 b Z_0]}{4[1-ab]^2 + [Z_0 a^2 b - 2Z_0 a - \frac{b}{Z_0}]^2} \tag{24a}$$

$$S_{21} = \frac{4[1-ab]}{4[1-ab]^2 + [Z_0 a^2 b - 2Z_0 a - \frac{b}{Z_0}]^2} - 2j \frac{[Z_0 a^2 b - 2Z_0 a - \frac{b}{Z_0}]}{4[1-ab]^2 + [Z_0 a^2 b - 2Z_0 a - \frac{b}{Z_0}]^2} \quad (24b)$$

and

$$Ang(S_{21}) = \tan^{-1}[-\frac{Z_0 a^2 b - 2Z_0 a - \frac{b}{Z_0}}{2(1-ab)}] \quad (24c)$$

$$\text{where } a = \frac{1-\omega^2 L_L C_R}{2\omega L_L} \text{ and } b = \frac{1-\omega^2 L_R C_L}{\omega C_L}$$

have been used in (24a)–(24c). As expressed in (20a)–(20d), the structural parameters of the CRLH TL unit cell can be used to determine the values of L_R, C_R, L_L and C_L and in turn to determine the phase incursion through (24c) and operation frequency through (24a) and (24b).

4.3 Designs of digital-phase shifters using CRLH unit cells

4.3.1 Basic ideas

The symmetrical CRLH TL unit cell in Fig. 12 (a) is used as the basic cell to design digital-phase shifters here. The advantage of using symmetrical CRLH TL unit cells is that when more unit cells are cascaded together to provide a more states, there is no need to perform any matching between adjacent unit cells.

Here, we use Fig.13 to illustrate our proposed idea of using CRLH TL unit cells to design digital-phase shifters. In the figure, we mount four switches on four different fingers of a unit cell. For an n-bit phase shifter, there will be a total of 2^n states, from 0 to 2^n-1, determined by "closed" or "open" states of the switches on the unit cell. The n-controlling bits are used to select a particular state from these 2^n-1 states and hence to provide a particular phase shift. The "closed" or "open" states in the switches determine the values L_R, C_R, L_L and C_L through (20a)-(20d) and, in turn, determine the phase incursion $Ang(S_{21})$ in (24c), so each switch state can be used to provide a particular phase shift, i.e.,

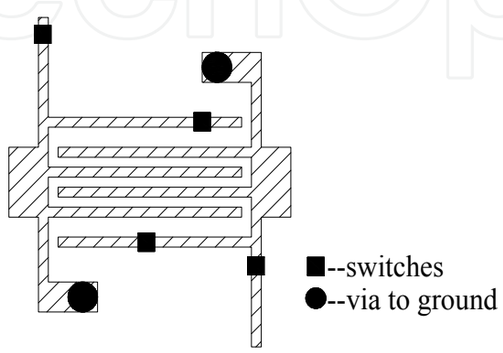

Fig. 13. Symmetrical CRLH TL unit cell mounted with four switches

$$\Delta\theta_m = Ang(S_{21})_m - Ang(S_{21})_0 \tag{25}$$

where m is the index (from 0 to 2^n-1) for the switch states, and $(S_{21})_m$ and $(S_{21})_0$ are the values of S_{21} in the m^{th}-switch and zeroth-switch states, respectively. For convenience and without lost of generality, the zeroth-switch state is taken as the state with all switches closed.

For high power applications such as radars, power-handling capability is one of the important concerns in the design of phase shifters. In our design, the power-handling capacity of the switches (i.e., PIN diodes in our case) used in the CRLH TL unit cell determines the power-handling capacity of the phase shifter. Here, surface-current density distribution is used to study the power-handling capacity of the switches. Computer simulation results on the surface-current density distribution of the CRLH TL unit cell on a Rogers substrate, RO5880, with eight fingers and four switches, are shown in Fig. 14. Figs. 14(a) and 14(b) show the surface-current density distributions with all four switches "opened" or "closed", respectively, at 9.5 GHz. The arrowheads indicate the positions of the switches on the fingers of the CRLH TL unit cell. With all switches "opened", Fig. 14 (a) shows that the largest surface-current density flowing through the switches is about -28 dB below (or 1/25.1 of) those flowing through the input and output ports. While with all switches "closed", Fig. 14 (b) shows that the largest surface-current density flowing through the switches is about -16 dB below (or 1/6.3 of) those flowing through the input and output ports. The width of the finger is only 1/7 of the port, so the largest surface-current through the switches is 16.43 dB below (or 1/44 of) those flowing through the ports. Thus the power-handling capability of the phase shifter is about 44 times higher than the power-handling capability of a switch (PIN diode).

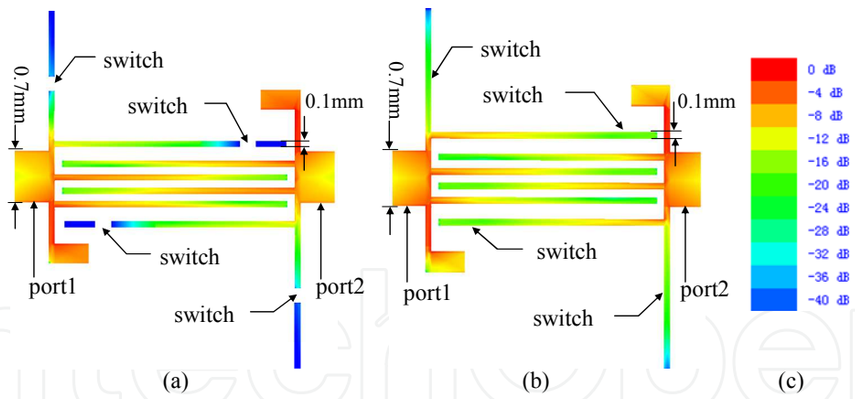

Fig. 14. Simulated surface-current density distribution on symmetrical CRLH TL unit cell with (a) all switches "opened", (b) all switches "closed", and (c) color scale

4.3.2 2-bit phase shifter

A 2-bit phase shifter using a single CRLH TL unit cell is shown in Fig. 15(a), where two switches are mounted on two different fingers (Zhang et al., 2010). The positions of the switches in the "open" and "close" states determine the values of L_R, C_R, L_L and C_L of the unit cell through (20a) – (20d) and hence the phase incursion. The state with all switches closed is taken as the zeroth-switch state. Simulation studies are used to determine the positions of the switches on the top and bottom fingers of the unit cell in order to achieve

the phase shifts of 45^0 and 22.5^0, respectively. The phase shifts of 67.5^0 and 0^0 are provided by "opening" and "closing", respectively, both two switches. Table 2 shows the phase shift for different input logic patterns. It should be noted that, although the phase shifts of 0^0, 22.5^0, 45^0 and 67.5^0 with equal step size of 22.5^0 are used in our design, other phase shift values and step sizes are just possible and easily be achieved. The layout of the 2-bit phase shifter with the DC bias circuits for the PINs (the switches) is shown in Fig. 15(b), where RF_{in} and RF_{out} are the input and output RF signals, respectively, and the input bits have the DC voltages of 0 and 5 V representing the two corresponding logic levels "1" and "0".

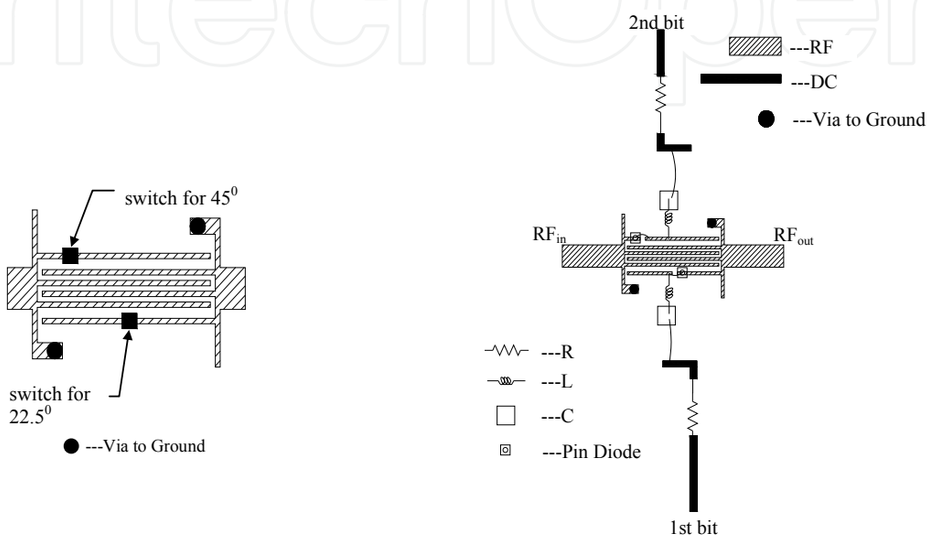

Fig. 15. (a) 2-bit phase shifter using CRLH TL unit cell and (b) layout of 2-bit phase shifter with DC bias circuits

States	Phase shifts
00	0^0
01	22.5^0
10	45^0
11	90^0

Table 2. Phase shifts for different states of 2-bit phase shifter

4.3.3 3-bit phase shifter

Fig. 16(a) shows a 3-bit phase shifter using a single CRLH TL unit cell where four switches are used to achieve eight different switch states and hence eight phase shifts of 0^0, 22.5^0, 45^0, 67.5^0, 90^0, 112.5^0, 135^0 and 157.5^0 (Zhang et al., 2010). Note that the number of controlling bits is less than the number of switches on the unit cell because two switches may be used to provide a phase shift. The state with all switches closed is taken as the zeroth-switch state. Again, computer simulation is used to determine the positions of these switches on the fingers in order to achieve these phase shifts. In Fig. 16(a), the two switches on the inner fingers are used to provide the phase shifts of 22.5^0 and 45^0. The two switches on the outer fingers serving in pair are used to provide a total phase shift of 90^0. Different switch states

are used to provide other phase shifts such as 67.5^0, 112.5^0, 135^0 and 157.5^0. When all switches are closed, the phase shift is 0^0. Table 3 shows the phase shift for different input logic pattern. The layout of the 3-bit phase shifter with DC bias circuit is shown in Fig. 16(b).

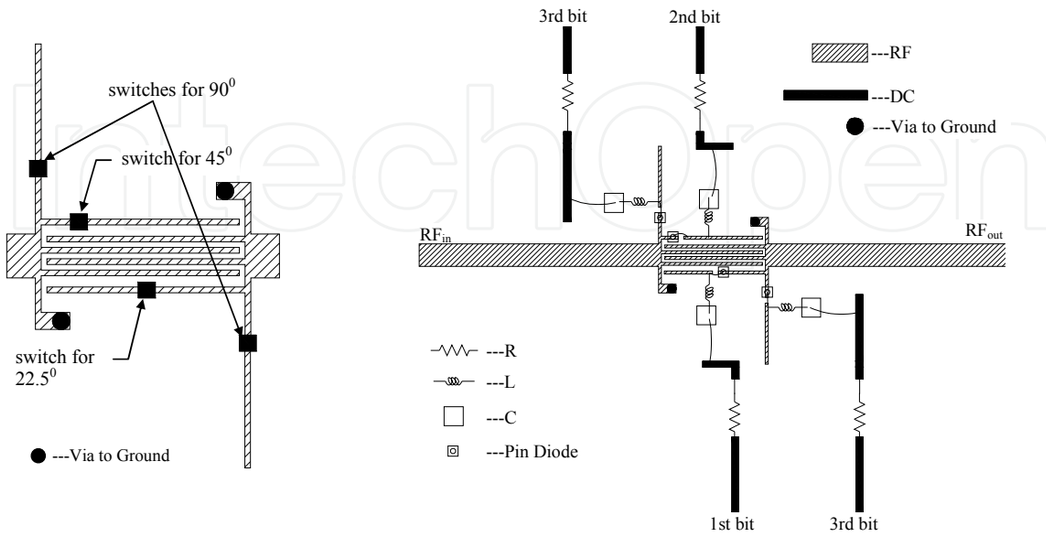

Fig. 16. (a) 3-bit phase shifter using one CRLH TL unit cell and (b) layout of 3-bit phase shifter with DC bias circuits

States	Phase shifts
000	0^0
001	22.5^0
010	45^0
011	67.5^0
100	90^0
101	112.5^0
110	135^0
111	157.5^0

Table 3. Phase shifts for different states of 3-bit phase shifter

4.3.4 6-bit phase shifter

To design a 6-bit phase shifter, we employ two symmetrical CRLH TL unit cells, as shown in Figs. 17(a) and 17(b), in cascade to provide the required phase shifts (Zhang et al., 2010). The state with all switches closed is taken as the zeroth-switch state. In the unit cell of Fig. 17(a), we use four switches to achieve sixteen different switch states and hence sixteen different phase shifts. The two switches on the inner fingers are used to provide the phase shifts of 5.625^0 and 11.25^0. The two switches on the outer fingers are used to provide the phase shifts of 22.5^0 and 45^0. Different switch states are used to provide other phase shifts such as 16.875^0, 28.125^0, 34.75^0, 39.375^0, 50.625^0, 56.25^0, 61.875^0, 67.5^0, 74.125^0,

78.75^0 and 84.375^0. Thus these switch states can be used to provide the phase shifts from 0^0 up to 84.375^0 at a step size of 5.625^0. In the unit cell of Fig. 17(b), we use two switches in a pair to provide the large phase shifts of 90^0 or 180^0. The pair of switches on the inner fingers provides a phase shift of 90^0, while the pair of switches on the outer fingers provides a phase shift of 180^0. The phase shift of 270^0 is achieved by "opening" all four switches. This phase shifter therefore can provide the phase shifts from 0^0 up to 270^0 at a step size of 90^0. By cascading these two unit cells, any phase shifts at a multiple number of 5.625^0 can be achieved by using the 6 controlling bits according to (25), i.e. the phase shifter can provide the phase shifts from 0^0 up to 354.375^0 at a step size of 5.625^0. Table 4 shows the phase shift for different input logic pattern. The layout of the 6-bit phase-shifter with DC bias circuits is shown in Fig. 17(c).

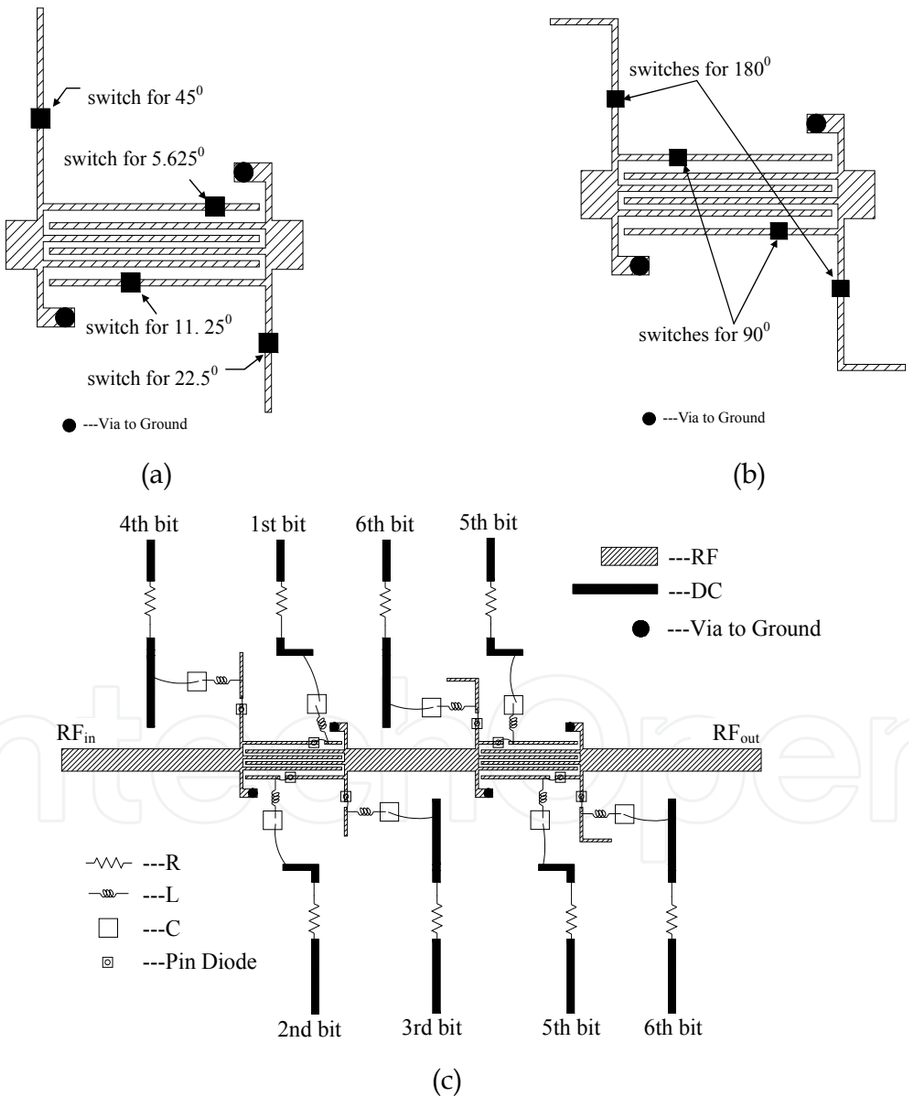

Fig. 17. 6-bit phase shifter using two CRLH TL unit cells. (a) CRLH unit cell in 1st stage, (b) CRLH unit cell in 2nd stage, and (c) layout of 6-bit phase shifter with DC bias circuits

States	Phase shifts	States	Phase shifts	States	Phase shifts	States	Phase shifts
000000	0^0	010000	90^0	100000	180^0	110000	270^0
000001	5.625^0	010001	95.625^0	100001	185.625^0	110001	275.625^0
000010	11.25^0	010010	101.25^0	100010	191.25^0	110010	281.25^0
000011	16.875^0	010011	106.875^0	100011	196.875^0	110011	286.875^0
000100	22.5^0	010100	112.5^0	100100	202.5^0	110100	292.5^0
000101	28.125^0	010101	118.125^0	100101	208.125^0	110101	298.125^0
000110	33.75^0	010110	123.75^0	100110	213.75^0	110110	303.75^0
000111	39.375^0	010111	129.375^0	100111	219.375^0	110111	309.375^0
001000	45^0	011000	135^0	101000	225^0	111000	315^0
001001	50.625^0	011001	140.625^0	101001	230.625^0	111001	320.625^0
001010	56.25^0	011010	146.25^0	101010	236.25^0	111010	326.25^0
001011	61.875^0	011011	151.875^0	101011	241.875^0	111011	331.875^0
001100	67.5^0	011100	157.5^0	101100	247.5^0	111100	337.5^0
001101	73.125^0	011101	163.125^0	101101	253.125^0	111101	343.125^0
001110	78.75^0	011110	168.75^0	101110	258.75^0	111110	348.75^0
001111	84.375^0	011111	174.375^0	101111	264.375^0	111111	354.375^0

Table 4. Phase shifts for different states of 6-bit phase shifter

4.4 Simulation and measurement results

The 2-bit, 3-bit and 6-bit phase shifters in Figs. 15(b), 16(b) and 17(c), respectively, have been designed to operate in an operating frequency band of 9-10 GHz using computer simulation. The substrates used in our designs were Rogers, RO5880, with a thickness of 0.254 mm and a permittivity of 2.2. The switches used were PIN diodes from SKYWORKS Co. Ltd, having a dimension of 0.35 mm×0.35 mm×0.15 mm, operating frequency range of 100 MHz-18 GHz and instantaneous power-handling capability of 2.5 W (34 dBm). Surface-mount-technology components such as resistors, capacitors and inductors were used to construct the bias circuits for the PIN diodes and also the circuits to isolate the RF signal from DC. For verification, all the final designs have been fabricated using Rogers substrate, RO5880, the same substrate used in our simulations. The prototyped modules of the *2*-bit, *3*-bit and *6*-bit phase-shifters are shown in Fig. 18, having the dimensions of 35 mm×40 mm×2 mm, 50 mm×40 mm×2 mm and 60 mm×40 mm×2 mm, respectively.

The return losses (-10log|S_{11}|), insertion losses (-10log|S_{21}|) and phase shifts of these prototyped phase shifters have been measured using a network analyzer to verify the simulation results. The simulation and measurement results for the *2*-bit, *3*-bit and *6*-bit phase shifters are shown in Figs. 19, 20 and 21, respectively. It can be seen that the simulated and measured results show good agreements.

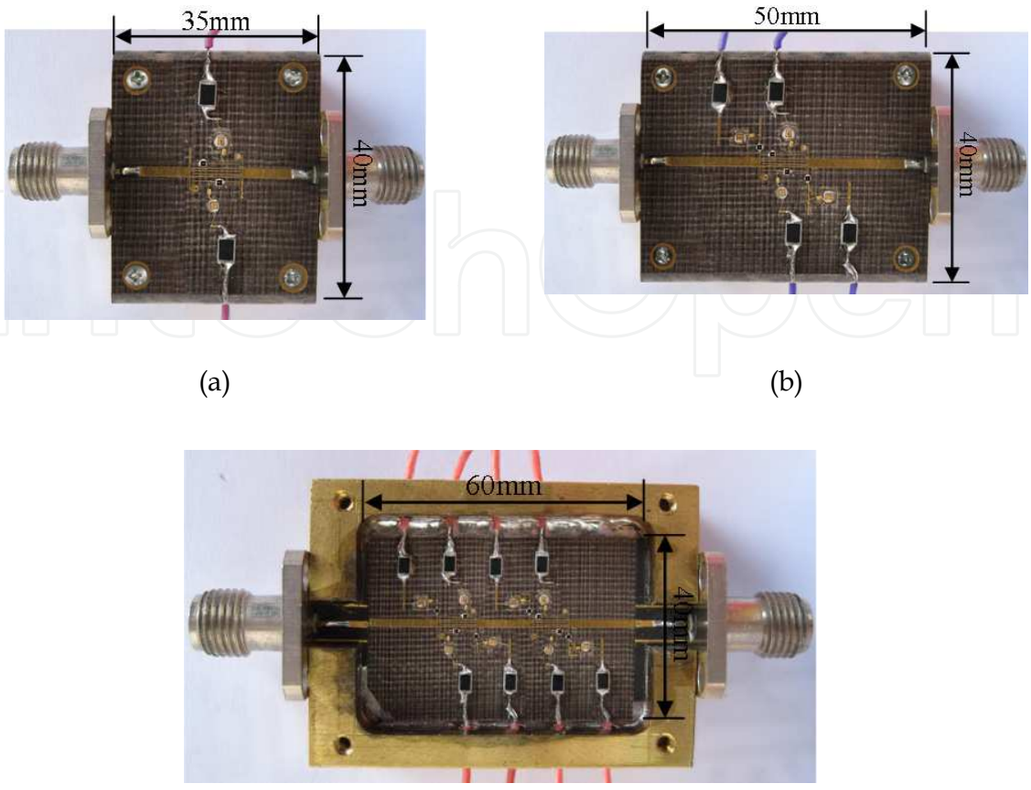

(a) (b)

(c)

Fig. 18. Prototyped (a) 2-bit phase shifter, (b) 3-bit phase shifter and (c) 6-bit phase shifter

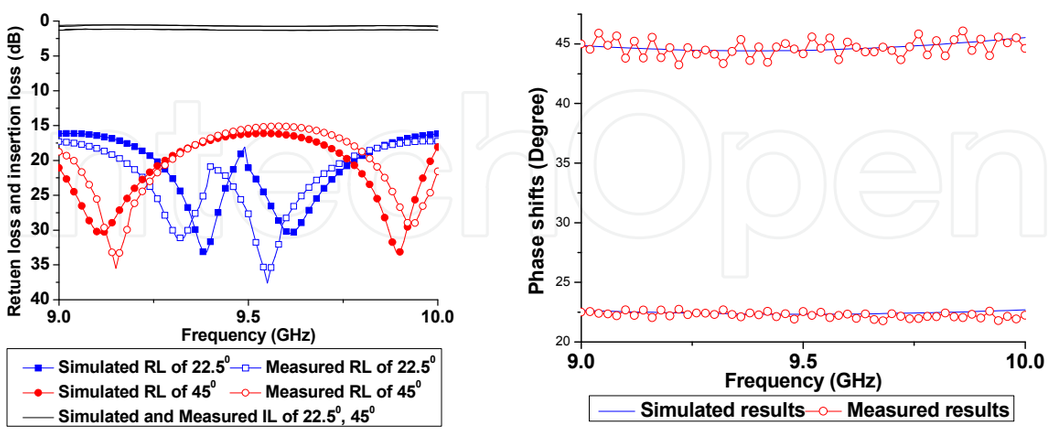

(a) (b)

Fig. 19. Simulated and measured results of 2-bit phase shifter; (a) return loss and insertion loss and (b) phase shift

The insertion losses of the three phase shifters are all less than 1.3 dB in the frequency band of 9-10 GHz. Figs. 19(a) and 20(a) show that the return losses of the 2-bit and 3-bit phase shifters are more than 15 dB in the frequency band of 9-10 GHz. For the 6-bit phase shifter, Fig. 21(a) shows the return loss is more than 15 dB for the frequency band from 9.2 to 9.8 GHz. Regarding accuracy, the measurement results in Fig. 19(b) show that the maximum error for the 2-bit phase shifter is about -2^0 at the phase shift of 67.5^0 and frequency of 9.73 GHz. For the 3-bit phase shifter, Fig. 20(b) shows that the maximum errors is $+4.5^0$ at the phase shift of 157.5^0 and frequency of 9.10 GHz. While for the 6-bit phase shifter, it is -6.3^0 at the phase shift of 180^0 and frequency of 9.66 GHz.

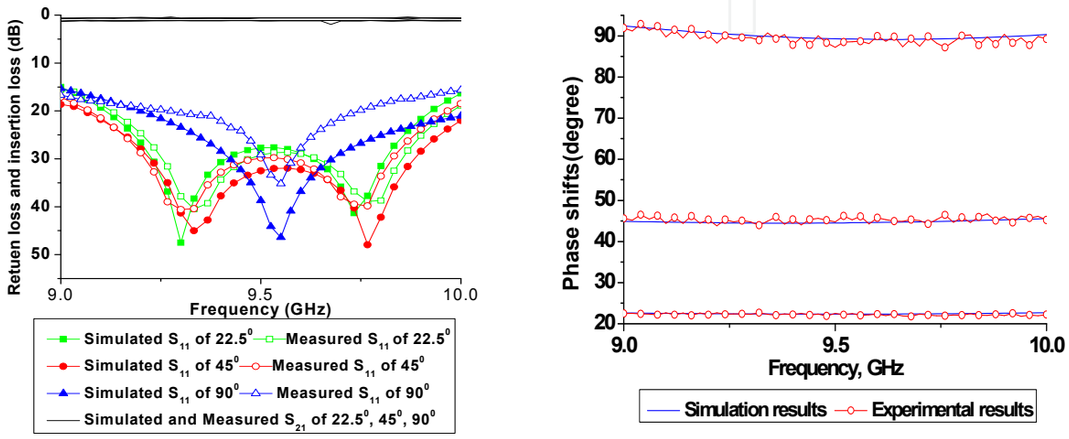

(a) (b)

Fig. 20. Simulated and measured results of 3-bit phase shifter; (a) return loss and insertion loss and (b) phase shift

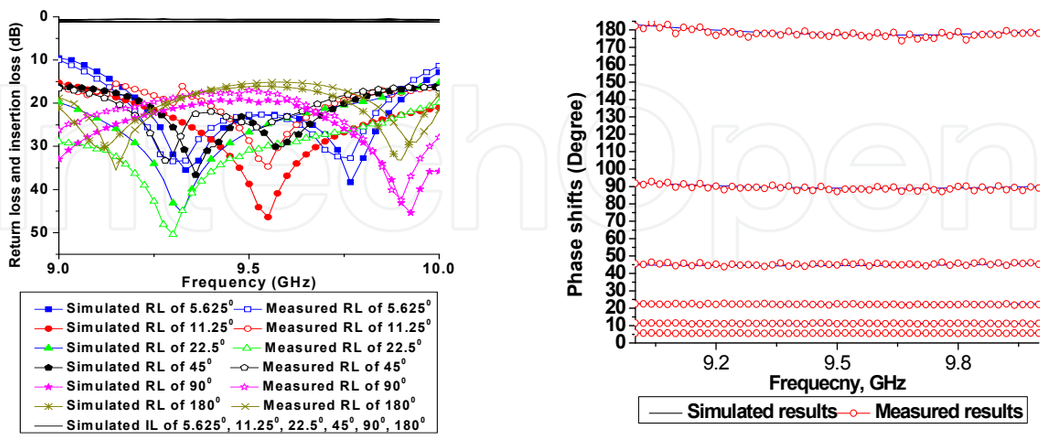

(a) (b)

Fig. 21. Simulated and measured results of 6-bit phase shifter; (a) return loss and insertion loss and (b) phase shift

The power-handling capability of the phase shifters has been studied using a setup with the block diagram shown in Fig. 22. The solid-state transmitter is basically an AM modulator which takes in the signal from the IF signal source, uses it to modulate the carrier signal at a much higher frequency and amplifies the modulated signal to a high-power level. The amplified signal is fed to the phase shifter under tested via an isolator which prevents any high-power signal from reflecting back and damaging the solid-state transmitter. A 40-dB coupler is used to couple a small portion of the high-power signal from the output of the phase shifter and feed it to the frequency spectrograph for measuring the power capability of the phase shifter. Majority of the high-power signal from the phase shifter is fed to a high-power load for power dissipation.

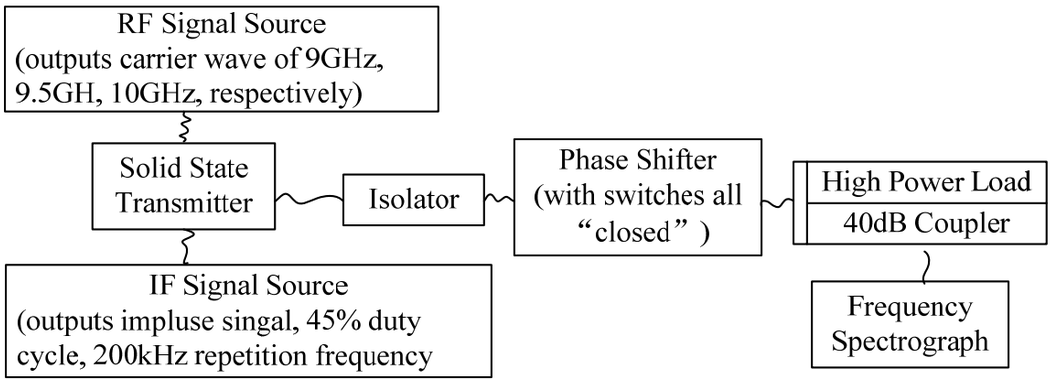

Fig. 22. Equipment setup for measuring power-handling capability of phase shifter

Frequency (GHz)		9	9.5	10
Peak Power (dBm)	2-bit	51.2	51.3	51.1
	3-bit	51.1	51.2	51.4
	6-bit	51.3	50.9	51.1

Table 5. Power-Handling Capability of Phase Shifters

In this study, the maximum transmitted peak power causing a diode to burn off is taken as the power-handling capability of the phase shifter and the results are shown in Table 5. Since the PIN diodes used in our design have an instantaneous power-handling capability of 34 dBm, the expected power-handling capabilities for the 2-bit, 3-bit and 6-bit phase shifters are about 50.43 dBm, i.e. 44 times higher as described previously. Table 4.4 shows that the power-handling capabilities of the three phase shifters at 9, 9.5 and 10 GHz are over 51.1, 51.1 and 50.9 dBm, respectively, corresponding to about 51.5, 51.5 and 49.2 times of the power-handling capability of the PIN diodes.

5. Conclusions

In this chapter, the EM metamatreials and the realization of EM metamaterials using the transmission line approach have been briefly described. A CRLH TL unit cell with a symmetrical structure has been proposed for the designs of TTDLs and digital-phase shifters. TTDLs using a single unit cell and four unit cells in cascaded have been designed and studied. Simulation and measurement results have shown that the TTDLs have the return losses of more than 15 dB and insertion losses of less than 1 dB. For the same length of 30 mm, the TTDL constructed using four CRLH TL unit cells in cascade can achieve a much larger TD, about 3.2 times larger, than that using the RH TL. Digital-phase shifters constructed using the CRLH TL unit cells have the advantages of small sizes, arbitrary phase-shift ranges and arbitrary step sizes. Three digital-phase shifters, 2-bit, 3-bit and 6-bit, have been designed and studied. Simulation and experimental results have shown that the digital-phase shifters have the low insertion losses of about 1.3 dB and return losses of larger than 15 dB across the operation bandwidths. Moreover, they have the much higher power-handling capabilities, about 50 times higher, than that of the PIN diodes used as switches in our designs for the digital-phase shifters.

6. References

Adam, J.D.; Davis, L.E.; Dionne, G.F.; Schloemann E.F. & Stitzer, S.N. (2002). Ferrite devices and materials. *IEEE Transactions on Microwave Theory and Techniques*, Vol. 50, 2002, pp. 721-737

Antoniades, M.A. & Eleftheriades, G.V. (2003). Compact linear lead/lag metamaterial phase shifters for broadband applications. *IEEE Antennas and Wireless Propagation Letters*, Vol. 2, 2003, pp.103-106

Bahl, I. (2011). *Lumped Elements for RF and Microwave Circuits*, Artech House, Boston& London

Caloz, C. & Itoh, T. (2006). *Electromagnetic Metamaterials: Transmission Line Theory and Microwave Applications: the Engineering Approach*, John Wiley & Sons, New Jersey

Damm, C.; Schüßler, M.; Freese J. & Jakoby, R. (2006). Artificial line phase shifter with separately tunable phase and line impedance, *36th European Microwave Conference*, 2006

Fetisov, Y.K. & Kabos, P. (1998). Active Magnetostatic Wave Delay Line. *IEEE Transactions on Magnetics*, Vol. 34, 1998, pp. 259 – 271

Keul, S. & Bhat, B. (1991). *Microwave and millimeter wave phase shifters*, Artech house, MA

Kim, H.; Kozyiev, A.B.; Karbassi, A. & van der Weide, D.W. (2005). Linear Tunable Phase Shifter Using a Left-handed Transmission-line. *IEEE Microwave and Wireless Components Letters*, Vol. 15, 2005, pp. 366-368

Kholodnyak, D.V.; Serebryakova, E.V.; Vendik, I.B. & Vendik, O.G. (2006). Broadband Digital Phase Shifter Based On Switchable Right- and Left-handed Transmission Line Sections. *IEEE Microwave and Wireless Components Letters*, Vol. 1, 2006, pp. 258-260

Kim, H. & Drayton, R.F. (2007). Size Reduction Method of Coplanar Waveguide (CPW) Electromagnetic Bandgap (EBG) Structures Using Slow Wave Design, *Topical Meeting on Silicon Monolithic Integrated Circuits in RF Systems*, 2007

Lai, A.; Itoh, T. & Caloz, C. (2004). Composite right/left-handed transmission line metamaterials. *IEEE Microwave Magazine*, Vol. 5, Sep 2004, pp. 34 – 50

Lee, T.H. (2004). *Planar Microwave Engineering*, Cambridge University Press, UK

Lapine, M.; Nefedov, I.S.; Saeily, J. & Tretyakov, S.A. (2006). Artificial lines with exotic dispersion for phase shifters and delay lines, *36th European Microwave Conference*, 2006

Marc, E.G. & Robert, A.P. (1991). Modelling Via Hole Grounds in Microstrip. *IEEE Microwave and Guided Wave Letters*, Vol. 1, 1991, pp. 135-137

Monti, G.; DePaolis, R. & Tarricone, L. (2009). Design of a 3-state reconfigurable CRLH transmission line based on MEMS switches, *Progress In Electromagnetics Research*, PIER 95, 2009, pp. 283-297

Pozar, M.D. (2004). *Microwave Engineering*, John Wiley & Sons, New Jersey

Rebeiz, G.M.; Tan, G.L. & Hayden, J.S. (2002). RF MEMS phase shifters: design and applications. *IEEE Microwave Magazine*, Vol. 2, 2002, pp. 72-81

Smith, W.R. & Gerard, H.M. (1969). Design of Surface Wave Delay Lines with Interdigital Transducers. *IEEE Transactions on Microwave Theory and Techniques*, Vol. 17, 1969, pp. 865 – 873

Ulaby, F.T. (2004). *Fundamentals of Applied Electromagnetics*, Pearson/Prentice Hall, New Jersey

Veselago, V.G. (1968). The electrodynamics of substances with simultaneously negative values of ε and μ, *Soviet Physics Uspekhi*, January-Feburary 1968

Vendik, I.B.; Kholodnyak, D.V. & Kapitanova, P.V. (2009). Microwave phase shifters and filters based on a combination of left-handed and right-handed transmission lines, In: *Metamaterials Handbook Vol. II. Applications of Metamaterials*, pp. 1-21, CRC Press

Woo, D.J.; Lee, J.W. & Lee, T.K. (2008). Multi-band Rejection DGS with Improved Slow-wave Effect, *38th European Microwave Conference*, 2008

Xu, J.; Lu, Z. & Zhang, X.C. (2004). Compact Involute Optical Delay Line. *Electronic Letters*, Vol. 40, 2004, pp. 1218 – 1219

Zhang, Y.Y. & Yang, H.Y.D. (2008). Ultra slow-wave periodic transmission line using 3D substrate metallization, *Microwave Symposium Digest 2008 IEEE MTT-S International*, 2008

Zhang, J.; Zhu, Q.; Jiang, Q. & Xu, S.J. (2009). Design of time delay lines with periodic microstrip line and composite right/left-handed transmission line. *Microwave and Optical Technology Letters*, Vol. 51, 2009, pp. 1679-1682

Zhang, J.; Cheung, S.W. & Yuk, T.I. (2010). Design of n-bit Phase Shifters with High Power Handling Capability Inspired by Composite Right/Left-handed Transmission Line Unit Cells. *IET Microwaves, Antennas & Propagation*, Vol. 4, August 2010, pp. 991-999

Zhang, J.; Cheung, S.W. & Yuk, T.I. (2010). A 3-bit Phase Shifter with High-power Capacity Based on Composite Right/Left-handed Transmission Line. *Microwave and Optical Technology Letters*, Vol. 52, August 2010, pp.1778-1782

Zhang, J.; Cheung, S.W. & Yuk, T.I. (2011). UWB True-time-delay Lines Inspired by CRLH TL Unit Cells. *Microwave and Optical Technology Letters*, Vol. 53, September 2011, pp.1955-1961

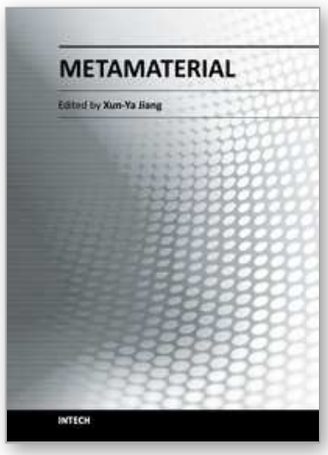

Metamaterial

Edited by Dr. Xun-Ya Jiang

ISBN 978-953-51-0591-6
Hard cover, 620 pages
Publisher InTech
Published online 16, May, 2012
Published in print edition May, 2012

In-depth analysis of the theory, properties and description of the most potential technological applications of metamaterials for the realization of novel devices such as subwavelength lenses, invisibility cloaks, dipole and reflector antennas, high frequency telecommunications, new designs of bandpass filters, absorbers and concentrators of EM waves etc. In order to create a new devices it is necessary to know the main electrodynamical characteristics of metamaterial structures on the basis of which the device is supposed to be created. The electromagnetic wave scattering surfaces built with metamaterials are primarily based on the ability of metamaterials to control the surrounded electromagnetic fields by varying their permeability and permittivity characteristics. The book covers some solutions for microwave wavelength scales as well as exploitation of nanoscale EM wavelength such as visible specter using recent advances of nanotechnology, for instance in the field of nanowires, nanopolymers, carbon nanotubes and graphene. Metamaterial is suitable for scholars from extremely large scientific domain and therefore given to engineers, scientists, graduates and other interested professionals from photonics to nanoscience and from material science to antenna engineering as a comprehensive reference on this artificial materials of tomorrow.

How to reference

In order to correctly reference this scholarly work, feel free to copy and paste the following:

J. Zhang, S.W. Cheung and T.I. Yuk (2012). Designs of True-Time-Delay Lines and Phase Shifters Based on CRLH TL Unit Cells, Metamaterial, Dr. Xun-Ya Jiang (Ed.), ISBN: 978-953-51-0591-6, InTech, Available from: http://www.intechopen.com/books/metamaterial/designs-of-true-time-delay-lines-and-phase-shifters-based-on-crlh-tl-unit-cells

INTECH
open science | open minds

InTech Europe
University Campus STeP Ri
Slavka Krautzeka 83/A
51000 Rijeka, Croatia
Phone: +385 (51) 770 447
Fax: +385 (51) 686 166
www.intechopen.com

InTech China
Unit 405, Office Block, Hotel Equatorial Shanghai
No.65, Yan An Road (West), Shanghai, 200040, China
中国上海市延安西路65号上海国际贵都大饭店办公楼405单元
Phone: +86-21-62489820
Fax: +86-21-62489821

IntechOpen